ISSN 1674-1056
http://cpb.iphy.ac.cn
http://iopscience.iop.org/cpb
中国物理 B
Chinese Physics
中国物理
Chinese Physics B

Bound states in the continuum on perfect conducting reflection gratings

Jianfeng Huang(黄剑峰), Qianju Song(宋前举), Peng Hu(胡鹏), Hong Xiang(向红), and Dezhuan Han(韩德专)
Citation: Chin. Phys. B, 2021, 30 (**8**): 084211. DOI: 10.1088/1674-1056/abeee4
Journal homepage: http://cpb.iphy.ac.cn; http://iopscience.iop.org/cpb

What follows is a list of articles you may be interested in

Three-dimensional spatial multi-point uniform light focusing through scattering media based on feedback wavefront shaping

Fan Yang(杨帆), Yang Zhao(赵杨), Chengchao Xiang(向成超), Qi Feng(冯祺), and Yingchun Ding(丁迎春)
Chin. Phys. B, 2021, 30 (**4**): 044207. DOI: 10.1088/1674-1056/abe3e6

Gain-induced large optical torque in optical twist settings

Genyan Li(李艮艳), Xiao Li(李肖), Lei Zhang(张磊), Jun Chen(陈君)
Chin. Phys. B, 2020, 29 (**8**): 084201. DOI: 10.1088/1674-1056/ab9616

Propagation properties of radially polarized Pearcey-Gauss vortex beams in free space

Xinpeng Chen(陈鑫鹏), Chuangjie Xu(许创杰), Qian Yang(杨芊), Zhiming Luo(罗智明), Xixian Li(李希贤), Dongmei Deng(邓冬梅)
Chin. Phys. B, 2020, 29 (**6**): 064202. DOI: 10.1088/1674-1056/ab8202

Trajectory engineering via a space-fractional Schrödinger equation with dynamic linear index potential

Yunji Meng(孟云吉), Youwen Liu(刘友文), Haijiang Lv(吕海江)
Chin. Phys. B, 2020, 29 (**5**): 054201. DOI: 10.1088/1674-1056/ab7b4c

Far-field vector-diffraction of off-axis parabolic mirror under oblique incidence

Xia-Hui Zeng(曾夏辉), Xi-Yao Chen(陈曦曜)
Chin. Phys. B, 2020, 29 (**3**): 034202. DOI: 10.1088/1674-1056/ab683e

---

SPECIAL TOPIC — Optical field manipulation

Bound states in the continuum on perfect conducting reflection gratings*

Jianfeng Huang(黄剑峰), Qianju Song(宋前举), Peng Hu(胡鹏), Hong Xiang(向红)†, and Dezhuan Han(韩德专)‡

College of Physics, Chongqing University, Chongqing 401331, *China*

(Received 5 February 2021; revised manuscript received 12 March 2021; accepted manuscript online 16 March 2021)

Bound states can be supported on the surface of a periodically corrugated perfect conductor known as spoof surface plasmon polaritons with their dispersion curves reside below the light line. Here we show that bound states in the continuum (BICs) can also be achieved in such systems. Two types of grating structures are proposed to suppress the radiation leakage and hence generate bound states. The first one is a simple grating with broad grooves in which multiple cavity modes are accommodated. Due to the symmetry incompatibility and the destructive interaction mainly from the TM_0 and TM_1 modes, BICs at the Γ point and at off-Γ points are both realized. The second one is a dimerized grating with two grooves in each unit cell. The destructive interaction between the modes in the two grooves can suppresses the radiation and BICs at the Γ point are observed. The Q factors of the whole bands can be further tuned by the dimerization strength effectively. This work may offer new opportunity for the applications of metallic grating in the low frequency bands.

Keywords: bound states in the continuum, perfect conducting grating, mode expansion method, spoof surface plasmon polaritons

PACS: 42.25.Fx, 42.25.Hz, 42.79.Dj, 73.20.Mf **DOI:** 10.1088/1674-1056/abeee4

1. Introduction

Electromagnetic (EM) states with high Q factors play important roles in photonics. In the high-Q states the EM field is confined to finite volume and the light–matter interaction is strongly enhanced, which is desirable for many applications such as optical modulators,[1] sensing,[2] laser,[3] and nonlinear optics.[4] Bound states with theoretically infinite high Q factors thus draw much attention in recent years. For periodic structures, bound states can be found in bands below the light line. Due to the photon momenta mismatch, the states below the light line cannot couple to the external radiation and then the EM fields are perfectly confined to the structure with infinite life time. Above the light line, the EM modes usually correspond to leaky resonances with finite lifetime. However, due to the symmetry incompatibility or destructive interaction between the radiation components, bound states can still be realized in this region. This is the bound states in the continuum (BICs). This concept was first proposed by von Neumann and Wigner in 1929[5] in quantum systems and later BICs have been revealed as a general wave phenomenon in many physical systems.[6–15,17] BICs in photonic systems have become an active research subject in recent years. The physical mechanism and properties of optical BICs have been studied extensively from the points view of vortex centers in the polarization direction of the radiation,[18] phase singularity of the quasi-mode coupling strength,[19,20] coherent perfect reflection of Bloch modes,[20–22] overlapping of multipolar singularities with open radiation channels,[23,24] etc. At the same time, many applications based on BICs were proposed and implemented.[25–30]

In research of BICs in photonic systems, most attention is paid to dielectric structures other than metallic ones in optical frequencies since the material loss for dielectrics is far less than that for metals. In the low frequencies, a metal can be treated as a perfect conductor and the material loss can be neglected, ensuring the possibility to generate BIC in metallic structures. However, related research for metallic system in low frequency regime is quite limited.[31] As the simplest system, metallic gratings are widely used and have been extensively investigated for spectral purpose. Besides, such structure can also support surface waves with the dispersion similar to that of the surface plasmon polaritons (SPPs), hence the name designer SPPs or spoof SPPs.[32,33] Spoof SPPs have found many applications in sensing, signal transmission and processing in the microwave and terahertz regimes.[34–38] If BICs can be realized on metallic grating structures, more applications are expected for these widely used devices in the low frequency regime.

To realize BICs in a periodic system, the basic idea is to introduce destructive interplays to suppress the total EM radiation. In this work, two strategies are proposed for the metallic

*Project supported by the National Natural Science Foundation of China (Grant No. 12074049) and the Fundamental Research Funds for the Central Universities, China (Grant Nos. 2020CDJQY-Z006 and 2019CDXZWL002).

†Corresponding author. E-mail: xhong@cqu.edu.cn

‡Corresponding author. E-mail: dzhan@cqu.edu.cn

© 2021 Chinese Physical Society and IOP Publishing Ltd

gratings. One is to accommodate multiple cavity modes in one groove by broadening the groove width. BIC can be achieved if the radiations from these modes superpose destructively so that the total radiation drops to zero. The other is to dimerize the grating so that there are two grooves in each unit cell. BICs are expected when the resonances in the two cavities interact destructively so that the total radiation diminishes to zero. Analytical method based on mode expansion is applied to calculate the dispersion and field distribution of the EM modes on the grating structures. For the grating with broad grooves, both the symmetry-protected BIC (SP-BIC) at the Γ point and the accidental BIC at the off-Γ point are observed by parameter tuning. For the dimerized grating, though only the SP-BIC is observed, the Q factors of the corresponding bands can be effectively tuned by the dimerization strength. The formation of BICs is explained theoretically and verified by the numerical simulation.

2. BICs on perfect conducting reflection grating with broad grooves

The perfect conducting grating under study is schematically shown in Fig. 1(a) as an inset. The structure is periodic in the x direction and uniform in y direction. The geometry is characterized by the period d, the groove width a, and the groove depth h. In this work, only the TM polarized modes are considered.

To analytically investigate the EM modes on the grating structure, the mode expansion method[39] is applied here. Considering the eigen-states (no external incidence) on the grating, the fields above the grating surface (region I) can be expressed as the sum of diffraction plane waves

$$\boldsymbol{E}^{\mathrm{I}}=\sum\rho_n\boldsymbol{E}^{\mathrm{dif},n},\quad \boldsymbol{H}^{\mathrm{I}}=\sum\rho_n\boldsymbol{H}^{\mathrm{dif},n}, \tag{1}$$

with

$$\boldsymbol{E}^{\mathrm{dif},n}=\frac{1}{\sqrt{d}}\mathrm{e}^{\mathrm{i}k_x^{(n)}x}\mathrm{e}^{-\mathrm{i}k_z^{(n)}z}\begin{pmatrix}1\\0\\k_x^{(n)}/k_z^{(n)}\end{pmatrix};$$

$$\boldsymbol{H}^{\mathrm{dif},n}=\frac{1}{\sqrt{d}}\mathrm{e}^{\mathrm{i}k_x^{(n)}x}\mathrm{e}^{-\mathrm{i}k_z^{(n)}z}\begin{pmatrix}0\\-k_0/k_z^{(n)}\\0\end{pmatrix}. \tag{2}$$

Here ρ_n is the diffraction coefficient, $k_x^{(n)}=k_x+2\pi n/d$, and $k_z^{(n)}=\sqrt{k_0^2-(k_x^{(n)})^2}$ with k_0 the wavenumber in free space and n an integer.

In the grooves (region II), the EM field can be expanded as the linear combination of the waveguide modes of different orders, TM_m, where m is an integer. For each m there are two degenerate waves propagating in opposite directions. Considering the perfect conducting boundary at the bottom of the groove, the superposition of the two TM_m modes gives rise to the following cavity mode:

$$\boldsymbol{E}^{\mathrm{cav},m}=\frac{1}{\sqrt{a}}\begin{pmatrix}\mathrm{i}\frac{\beta^{(m)}}{k}\cos\left[\frac{m\pi}{a}(x-\frac{a}{2})\right]\sin[\beta^{(m)}(z-h)]\\0\\-\mathrm{i}\frac{m\pi}{ka}\sin\left[\frac{m\pi}{a}(x-\frac{a}{2})\right]\cos[\beta^{(m)}(z-h)]\end{pmatrix},$$

$$\boldsymbol{H}^{\mathrm{cav},m}=\frac{1}{\sqrt{a}}\begin{pmatrix}0\\\cos\left[\frac{m\pi}{a}(x-\frac{a}{2})\right]\cos\left[\beta^{(m)}(z-h)\right]\\0\end{pmatrix}, \tag{3}$$

where $\beta^{(m)}=\sqrt{k_0^2-(\frac{m\pi}{a})^2}$.

Then the fields in the grooves can be expressed as

$$\boldsymbol{E}^{\mathrm{II}}=\sum_{m=0}^{\infty}C_m\boldsymbol{E}^{\mathrm{cav},m},\quad \boldsymbol{H}^{\mathrm{II}}=\sum_{m=0}^{\infty}C_m\boldsymbol{H}^{\mathrm{cav},m}. \tag{4}$$

The boundary condition requires the continuity of E_x at $z=0$ over the whole unit cell and the continuity of H_y at $z=0$ in the groove area. By matching the boundary condition the coefficients above are connected as

$$\rho_n=-\mathrm{i}\sqrt{\frac{a}{d}}\sum_{m\geq0}C_m\frac{\beta^{(m)}}{k}\sin(\beta^{(m)}h)V_{nm}, \tag{5}$$

$$C_m=\frac{1}{\cos(\beta^{(m)}h)}\sqrt{\frac{a}{d}}\sum_{n=-\infty}^{\infty}r_n\frac{-k}{k_z^{(n)}}W_{nm}, \tag{6}$$

where

$$V_{nm}=\frac{1}{2}\mathrm{e}^{\mathrm{i}m\pi/2}\mathrm{sinc}\left(k_x^{(n)}a/2+m\pi/2\right)+\frac{1}{2}\mathrm{e}^{-\mathrm{i}m\pi/2}\mathrm{sinc}\left(k_x^{(n)}a/2-m\pi/2\right),$$

$$W_{nm}=\begin{cases}\mathrm{sinc}(k_x^{(n)}a/2), & m=0,\\ \mathrm{e}^{-\mathrm{i}m\pi/2}\mathrm{sinc}(k_x^{(n)}a/2+m\pi/2)+\mathrm{e}^{\mathrm{i}m\pi/2}\mathrm{sinc}(k_x^{(n)}a/2-m\pi/2), & m>0.\end{cases}$$

Submitting Eq. (5) into Eq. (6), the equations about C_m are obtained as

$$C_m=\sum_{n\geq0}L_{mn}C_n, \tag{7}$$

where $L_{mn}=\mathrm{i}\frac{a}{d}\frac{\sin(\beta^{(n)}h)}{\cos(\beta^{(m)}h)}\beta^{(n)}\sum_{l=-\infty}^{\infty}\frac{1}{k_z^{(l)}}W_{lm}V_{ln}$.

The dispersion can be obtained by the solvability condition of Eq. (7) as

$$\det\left[L_{mn}-\delta_{mn}\right]=0. \tag{8}$$

And then the coefficients ρ_n and C_m can be determined up to an arbitrary common scale factor.

For grating with groove width $a<d/2$, in the 0^{th}-order region, there is only one propagating waveguide mode (TM_0) in the grooves, since the cutoff frequency of the TM_1 mode,

π/a, is always larger than the highest frequency of the 0$^{\text{th}}$-order region ($2\pi/d$). The corresponding EM field in the grating grooves is dominated by the TM_0 mode which can strongly couple to the external radiation, hence no BIC forms.

Increasing the groove width so that $a > d/2$, for certain bands there are two propagating modes (TM_0 and TM_1) in each groove and the high-order ones are evanescent. As the two modes can serve as comparable radiation sources, it is possible to suppress the radiation and further achieve BICs by means of destructive interference via the parameter tuning.

Figure 1 shows the calculated band diagram and the corresponding Q factors when the first few cavity modes are considered. The simulated results are also presented. For the dispersion, the analytical results with different numbers of modes taken into account exhibit negligible difference, even only the TM_1 mode is considered. While for the Q factors, the results show remarkable dependence on the number of modes. If only the TM_1 mode is considered, the off-Γ BIC won't appear. When the first two (TM_0 and TM_1) modes are considered, both the at-Γ BIC and the off-Γ BIC appear. With more modes taken into account, the analytical results show better agreement with that of the simulation. When the first seven modes (TM_0 to TM_6) are considered, the analytical result highly coincides with the simulation.

The above results can be explained by examining the modes in the grooves and the diffraction coefficient ρ_0. As there is only one radiation channel in the 0$^{\text{th}}$-order region, the radiation leakage, and hence the Q factors of the EM mode can be reflected by ρ_0. The following discuss is based on the analytical result with the first seven modes considered. The relative magnitudes of the cavity modes C_m/C_1 ($m = 0$, 2, 3, 4, 5, 6) for the current structure are calculated and shown in Fig. 2(a). It is obvious that the TM_1 mode dominates the whole band. The magnitudes of the other modes are several orders of magnitudes smaller than that of TM_1, and the higher the order is, the smaller the magnitude is. At the Γ-point, there is purely a TM_1 mode and hence a SP-BIC appears here due to the symmetry incompatibility. At the off-Γ BIC point, the TM_1 mode is still dominant and the field profile shown in Fig. 1(b) still exhibits an anti-symmetric feature.

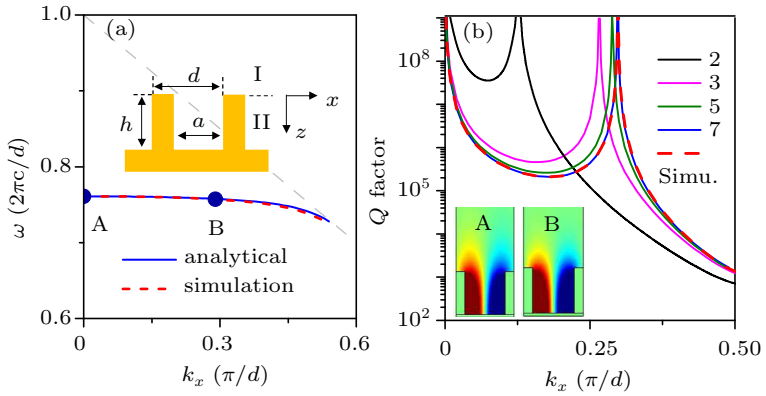


Fig. 1. Dispersion (a) and the Q factors (b) of the interested band. The analytical results for the dispersions with different numbers of modes considered are almost the same. The analytical results of the Q factors with different numbers of modes considered are presented in (b). The inset in panel (a) indicates the geometry of the grating. The insets in panel (b) are the magnetic field profiles (H_y) corresponding to the two BIC points marked in the band diagram with "A" and "B" in (a). Note that the profile correspond to B looks antisymmetric due to the dominance of the TM_1 mode. Here the geometry parameters are set as $a = 3.5$ mm, $h = 3.75$ mm, and $d = 5$ mm.

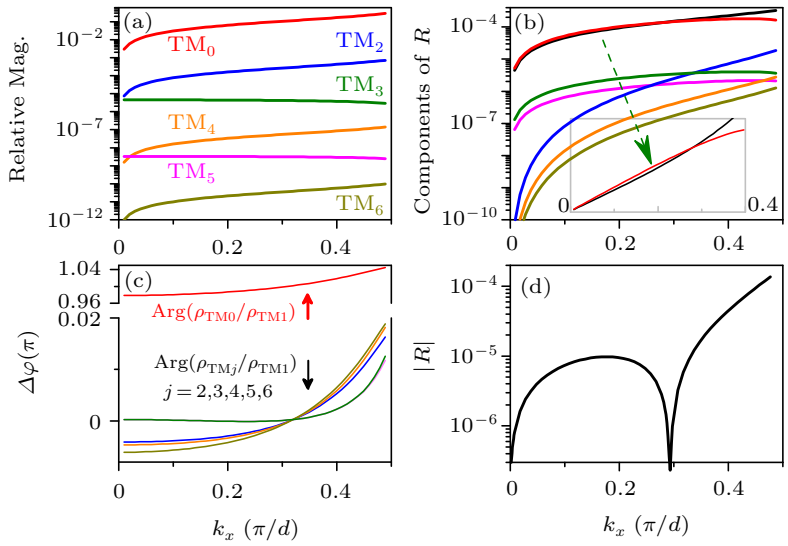


Fig. 2. (a) The relative magnitude of the cavity modes with respect to TM_1. (b) The magnitude of the radiation components R_{TMj} ($j = 0, 1 \ldots, 6$). The inset in (b) shows R_{TM0} and R_{TM1} in linear coordinates. (c) The phase difference between R_{TMj} ($j = 0, 2 \ldots, 6$) and R_{TM1}. The mapping of the colors to the cavity modes in (b) and (c) is the same as that in (a). (d) The sum of the radiation components (see Eq. (9)).

According to Eq. (5), each EM mode in the grooves contributes to the radiation. For the sake of brevity hereafter ρ_0 is denoted as R, that is, $R \equiv \rho_0$. When the first seven modes are considered Eq. (5) can be conveniently rewritten as

$$R = R_{\mathrm{TM0}} + R_{\mathrm{TM1}} + \cdots + R_{\mathrm{TM6}}. \tag{9}$$

As displayed in Fig. 2(b), the radiation from the first two modes, R_{TM0} and R_{TM1}, is much higher than that from the other high order modes. Meanwhile, R_{TM0} and R_{TM1} are comparable in magnitude. The phase differences between $R_{\mathrm{TM}j}$ ($j = 0,2,3,4,5,6$) and R_{TM1} are shown in Fig. 2(c). It can be seen that the components $R_{\mathrm{TM}j}$ ($j = 1,2,\ldots,6$) are almost in phase while R_{TM0} is nearly π radians out of phase with the other components. Combing Figs. 2(b) and 2(c), one can see that the high Q factors mainly come from the destructive interaction of the TM_0 and TM_1 modes, and the high-order modes provide some corrections to the Q factors. Adding up all the components the diffraction coefficient R is obtained, as shown in Fig. 2(d). The two dips indicate the vanishing of radiation, that is, the existence of BICs, and the positions of the dips are highly consistent with the peaks of the simulated Q factors shown in Fig. 1(b).

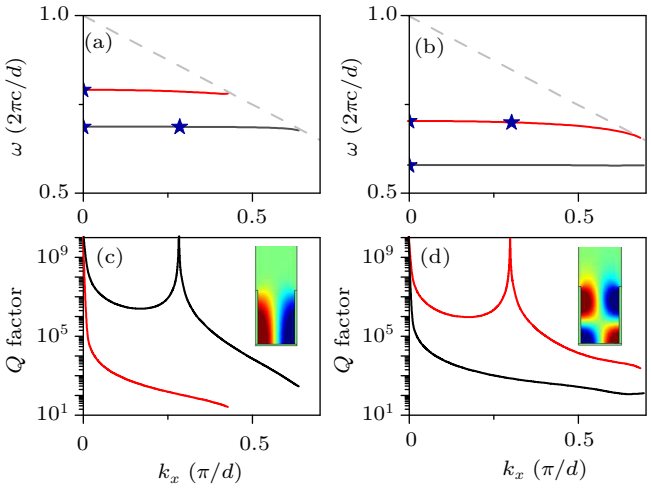


Fig. 3. Band diagrams and the corresponding Q factors of two grating structures with $d = 5$ mm and $h = 8$ mm. (a) and (c) correspond to the groove width $a = 4.46$ mm; (b) and (d) correspond to $a = 3.72$ mm. The stars in the band diagrams indicate the position of BICs. The insets are the magnetic field (H_y) profiles correspond to the lower (c) and upper (d) bands at the Γ points, respectively.

The band discussed above actually corresponds to the fundamental longitudinal mode in the grating grooves. Increasing the groove depth, high-order longitudinal resonance in the z direction can be further supported and accordingly more bands will appear in the 0^{th}-order region. By tuning the geometry parameters, BICs can also be generated in these bands. Figure 3 shows the simulated band diagrams and the corresponding Q factors on two gratings with deeper grooves ($h = 8$ mm). The lower band corresponds to the fundamental (0^{th}-order) longitudinal mode and the upper band corresponds to the 1^{st}-order longitudinal mode, which are characterized by the number of nodes in the field profiles along the z direction. The SP-BICs at the Γ-points are always supported and the off-Γ BIC can be supported on either band by tuning the groove width.

3. High Q modes and BICs on dimerized perfect reflection conducting gratings

The dimerized grating under study is schematically shown in Fig. 4 as an inset above panel (e). In each unit cell there are two identical grooves with width a and depth h. The two grooves are separated by a ridge with width of b, and the period of the grating is d. In this work, only the TM polarized modes are considered.

The EM modes on the dimerized grating can be analytically solved with the method applied in Section 1. The field above the grating surface (region I) is still expressed as the sum of diffraction plane waves. In the grooves (region II), the EM field is expanded as the linear combination of the cavity modes. For the dimerized grating considered here, the groove width $a < d/2$ and hence the cutoff frequency of the TM_1 mode are beyond the 0th-order region. As we focus on the modes in the 0^{th}-order region, only the fundamental waveguide mode in the groove is considered. Then the fields in the left-hand-side and right-hand-side grooves can be expressed respectively as

$$\boldsymbol{E}_{\mathrm{L}}^{\mathrm{II}} = C_{0,\mathrm{L}}\boldsymbol{E}^{\mathrm{cav},0}, \quad \boldsymbol{H}_{\mathrm{L}}^{\mathrm{II}} = C_{0,\mathrm{L}}\boldsymbol{H}^{\mathrm{cav},0}, \tag{10}$$

$$\boldsymbol{E}_{\mathrm{R}}^{\mathrm{II}} = D_{0,\mathrm{R}}\boldsymbol{E}^{\mathrm{cav},0}, \quad \boldsymbol{H}_{\mathrm{R}}^{\mathrm{II}} = D_{0,\mathrm{R}}^{\mathrm{cav},0}. \tag{11}$$

By matching the boundary condition the coefficients above can be solved as

$$\begin{aligned}\frac{C_{0,\mathrm{R}}}{C_{0,\mathrm{L}}} &= -\frac{\sum_{n=-\infty}^{\infty}\mathrm{sinc}^2(k_x^{(n)}\frac{a}{2})\frac{k_0}{k_z^{(n)}} + \mathrm{i}\frac{d}{a}\cot(k_0 h)}{\sum_{n=-\infty}^{\infty}\mathrm{sinc}^2(k_x^{(n)}\frac{a}{2})\frac{k_0}{k_z^{(n)}}\mathrm{e}^{-\mathrm{i}k_x^{(n)}(a+b)}} \\ &= -\frac{\sum_{n=-\infty}^{\infty}\mathrm{sinc}^2(k_x^{(n)}\frac{a}{2})\frac{k_0}{k_z^{(n)}}\mathrm{e}^{\mathrm{i}k_x^{(n)}(a+b)}}{\sum_{n=-\infty}^{\infty}\mathrm{sinc}^2(k_x^{(n)}\frac{a}{2})\frac{k_0}{k_z^{(n)}} + \mathrm{i}\frac{d}{a}\cot(k_0 h)};\end{aligned} \tag{12}$$

$$\begin{aligned}\rho_m &= \left(1-\mathrm{e}^{\mathrm{i}2\beta^{(0)}h}\right)\sqrt{a/d}\mathrm{sinc}(k_x^{(m)}a/2) \\ &\quad\times\left[C_{0,L}\mathrm{e}^{\mathrm{i}k_x^{(m)}(a+b)/2} + C_{0,R}\mathrm{e}^{-\mathrm{i}k_x^{(m)}(a+b)/2}\right].\end{aligned} \tag{13}$$

And the dispersion, based on Eq. (12), can be obtained as

$$\begin{aligned}&\left[\sum_{n=-\infty}^{\infty}\mathrm{sinc}^2(k_x^{(n)}\frac{a}{2})\frac{k_0}{k_z^{(n)}} + \mathrm{i}\frac{d}{a}\cot(k_0 h)\right]^2 \\ &= \sum_{n=-\infty}^{\infty}\mathrm{sinc}^2\left(k_x^{(n)}\frac{a}{2}\right)\frac{k_0}{k_z^{(n)}}\mathrm{e}^{-\mathrm{i}k_x^{(n)}(a+b)} \\ &\quad\times\sum_{m=-\infty}^{\infty}\mathrm{sinc}^2\left(k_x^{(m)}\frac{a}{2}\right)\frac{k_0}{k_z^{(m)}}\mathrm{e}^{\mathrm{i}k_x^{(m)}(a+b)}.\end{aligned} \tag{14}$$

Figure 4(a) shows the dispersions of the EM modes on a dimerized grating with $d = 10$ mm, $h = 7$ mm, $a = 2$ mm, $b = 2$ mm. Below the light line there are two spoof SPPs bands

with a gap between them. As the two bands reside below the light line, their Q factors are infinitely high. There are two bands (1 and 2) in the 0$^{\text{th}}$-order region and the corresponding Q factors are presented in Fig. 4(b). The Q factors for both branches are very high and diverge at the Γ point, manifesting the existence of BICs. This can be further confirmed by the corresponding field profiles shown in Fig. 4(b) as insets, in which the fields are confined to the grating with antisymmetric distribution in the x direction, manifesting the characteristic of the SP-BICs.

As mentioned in Section 1, the radiation leakage in the 0$^{\text{th}}$-order region can be reflected by the diffraction coefficient ρ_0. According to Eq. (13),

$$\rho_0 \propto \left[C_{0,\mathrm{L}}\, \mathrm{e}^{\mathrm{i}k_x(a+b)/2} + C_{0,\mathrm{R}}\, \mathrm{e}^{-\mathrm{i}k_x(a+b)/2}\right], \qquad (15)$$

where $C_{0,\mathrm{L}}$ and $C_{0,\mathrm{R}}$ are the magnitude of modes in the two grooves and $k_x(a+b)$ is the Bloch phase difference between the two grooves in a unit cell. The relative magnitude, $|C_{0,\mathrm{R}}/C_{0,\mathrm{L}}|$, and phase difference, $\Delta\varphi = \mathrm{Arg}(C_{0,\mathrm{R}}/C_{0,\mathrm{L}}) - k_x(a+b)$, of the two terms in Eq. (15) are plotted in Figs. 4(c) and 4(d). At the Γ point, for both bands, EM modes in the two grooves oscillate with the same magnitude and π radians phase difference, and hence symmetry-protected BICs form here. Away from the Γ point, the relative magnitudes deviate from 1 and the phase differences deviate from π radians, thus the radiation cannot be canceled out and no BIC forms. Actually, no off-Γ point BIC is observed for the dimerized grating, in spite of fine parameter tuning. It is also worth noting that with the increase of k_x, the Q factors of the two bands decrease first and then increase, which is consistent with the variation of the relative magnitude shown in Fig. 4(c).

The Q factors of the whole bands can be modulated by the dimerization strength. Here the dimerization strength can be defined by $S = |(a+b)/d - 1/2|$, with larger S indicating stronger dimerization. Figure 4(e) shows the Q factors of bands 1 and 2 with different dimerization strengths. Here for the three structures, b is set as 2 mm, 2.5 mm, and 2.9 mm, respectively, and the other parameters are fixed as $d = 10$ mm, $h = 7$ mm, and $a = 2$ mm. For the three structures, smaller b corresponds to stronger dimerization. It is apparent that the Q factors of the two bands increase as a whole with the decrease of the dimerization strength.

When the dimerization strength$S$ decreases to 0, the dimerized grating degenerates into to a simple grating with period of $d/2$ and there is only one groove in each unit cell. In this case the band diagram is changed and there are two spoof SPPs bands residing below the light line, as shown in Fig. 5(a). Previous bands 1 and 2 turn into parts of the spoof SPPs bands. In fact, bands 1 and 2 are the results of the band folding of spoof SPPs due to the lattice dimerization. When a uniform single "atom" lattice is dimerized (here corresponding to the periodically perturbation of the spacing between two neighboring grooves), the period of the lattice is doubled. Therefore, the original Brillouin zone is halved in size and part of the original bands fold back into the new Brillouin zone, forming the bands of 1 and 2, as shown in Fig. 5(b). Since bands 1 and 2 are evolved from the spoof SPPs, the high Q property is inherited, and the weaker the dimerization is, the higher Q values the bands have. Thus lattice dimerization provides a convenient way to achieve high Q modes.

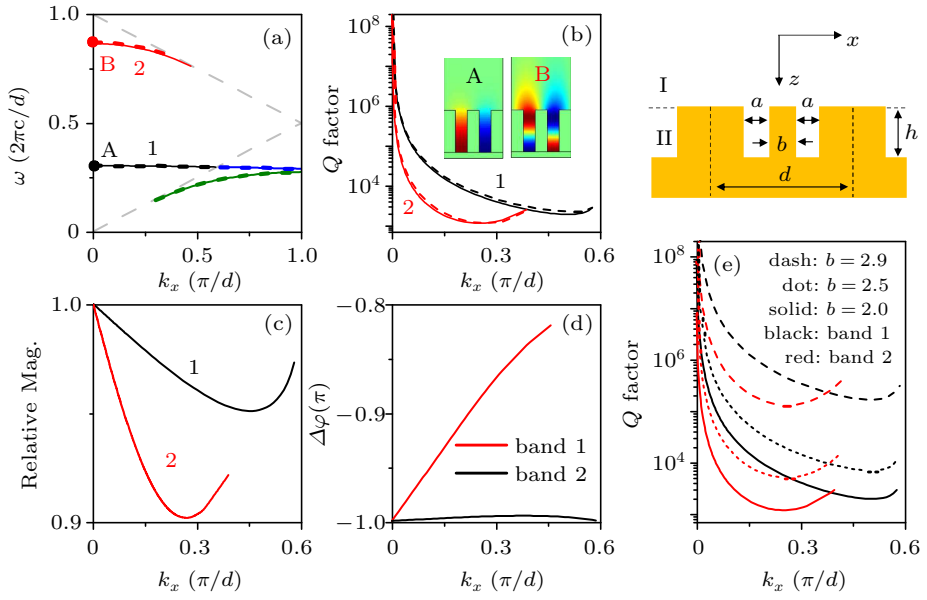


Fig. 4. (a) Band diagram and Q factors for the TM modes on the dimerized grating, with the solid lines for simulation and dash lines for analytical results. The two bands below the light line correspond to the spoof SPPs. The geometry of the grating is shown as an inset above panel (e). (b) The Q factors for band 1 and 2, with the dash lines for simulation and solid lines for analytical results. The insets are the field profiles (H_y) corresponding to points A and B marked in (a). (c) Relative magnitude of the modes in two grooves for bands 1 and 2. (d) Phase difference between the modes in the two grooves, with $\Delta\varphi = \mathrm{Arg}(C_{0,\mathrm{R}}/C_{0,\mathrm{L}}) - k_x(a+b)$. The geometry parameters for (a)–(d) are $d = 10$ mm, $h = 7$ mm, $a = 2$ mm, $b = 2$ mm. (e) The Q factors for gratings with different dimerization strength. Here smaller b corresponds to stronger dimerization.

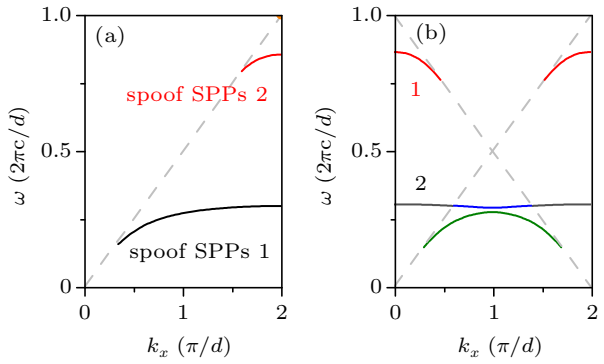


Fig. 5. Band diagrams for the non-dimerized (a) and dimerized (b) gratings. The band diagram of (b) can be regarded as the result of band folding of diagram (a).

4. Conclusions

Bound states in the continuum are realized on two types of perfect conducting gratings. The first structure is a simple grating with groove width larger than half of the period, in which both the SP-BIC at the Γ-point and an off-Γ BIC are observed. The analytical result shows that in such a system, the TM_0 and TM_1 modes serve as two comparable radiation sources, and the off-Γ BIC is formed when destructive interaction between the two modes happens. The second structure is a dimerized grating in which radiation from the two grooves can interfere destructively and SP-BICs are observed. In addition, the Q factors of the whole band can be tuned effectively by the strength of the dimerization.

The structures proposed here are easy to fabricate and hence can provide a platform for BIC research. In addition to the spoof SPPs supported on such grating structures, the high Q EM modes and the BICs discussed here may find more applications for the metallic gratings in the low frequency bands.

References

[1] Melikyan A, Alloatti L and Muslija A 2014 *Nat. Photon.* **8** 229
[2] Liu N, Tang M L, Hentschel M, Giessen H and Alivisatos A P 2011 *Nat. Mater.* **10** 631
[3] Noda S 2010 *JOSA B* **27** B1
[4] Corcoran B, Monat C and Grillet C 2009 *Nat. Photon.* **3** 206
[5] Von Neumann J and Wigner E 1929 *Phys. Z* **30** 465
[6] Friedrich H and Wintgen D 1985 *Phys. Rev. A* **32** 3231
[7] Bulgakov E and Sadreev A 2011 *Phys. Rev. B* **83** 235321
[8] Zhang J M, Braak D and Kollar M 2012 *Phys. Rev. Lett.* **109** 116405
[9] Molina M I, Miroshnichenko A E and Kivshar Y S 2012 *Phys. Rev. Lett.* **108** 070401
[10] Linton C M and McIver P 2007 *Wave Motion* **45** 16
[11] Marinica D C, Borisov A G and Shabanov S V 2008 *Phys. Rev. Lett.* **100** 183902
[12] Bulgakov E N and Sadreev A F 2008 *Phys. Rev. B* **78** 075105
[13] Plotnik Y, Peleg O, Dreisow F, Heinrich M, Nolte S, Szameit A and Segev M 2011 *Phys. Rev. Lett.* **107** 183901
[14] Hsu C W, Zhen B, Stone A D, Joannopoulos J D and Soljačić M 2016 *Nat. Rev. Mater.* **1** 16048
[15] He Y, Guo G, Feng T, Xu Y and Miroshnichenko A E 2018 *Phys. Rev. B* **98** 161112
[16] Chen G Y, Zhang W X and Zhang X D 2019 *Opt. Express* **27** 16449
[17] Yang Y, Peng C, Liang Y, Li Z and Noda S 2014 *Phys. Rev. Lett.* **113** 037401
[18] Zhen B, Hsu C W, Lu L, Stone A D and Soljačić M 2014 *Phys. Rev. Lett.* **113** 257401
[19] Bulgakov E N and Maksimov D N 2017 *Phys. Rev. Lett.* **118** 267401
[20] Song Q J, Zhao M X, Liu L, Chai J W, He G H, Xiang H, Han D Z and Zi J 2019 *Phys. Rev. A* **100** 023810
[21] Dai S W, Liu L, Han D Z and Zi J 2018 *Phys. Rev. B* **98** 081405
[22] Song Q J, Hu J S, Dai S W, Zheng C X, Han D Z, Zi J, Zhang Z Q and Chan C T 2020 *Sci. Adv.* **6** eabc1160
[23] Chen W, Chen Y and Liu W 2019 *Phys. Rev. Lett.* **122** 153907
[24] Sadrieva Z, Frizyuk K, Petrov M, Kivshar Y and Bogdanov A 2019 *Phys. Rev. B* **100** 115303
[25] Foley J M, Young S M and Phillips J D. 2014 *Phys. Rev. B* **89** 165111
[26] Kodigala A, Lepetit T, Gu Q, Bahari B, Fainman Y and Kanté B 2017 *Nature* **541** 196
[27] Liu Y, Zhou W and Sun Y 2017 *Sensors* **17** 1861
[28] Bulgakov E N and Sadreev A F 2014 *Opt. Lett.* **39** 5212
[29] Bulgakov E N and Sadreev A F 2017 *Phys. Rev. A* **96** 013841
[30] Koshelev K, Sychev S, Sadrieva Z, Bogdanov A and Iorsh I 2018 *Phys. Rev. B* **98** 161113
[31] Zhang W, Charous A, Nagai M, Mittleman D M and Mendis R 2018 *Optics express* **26** 13195
[32] Pendry J B, Martín-Moreno L and García-Vidal F J 2004 *Science* **305** 847
[33] Hibbins A P, Evans B R and Sambles J R 2005 *Science* **308** 670
[34] Williams C R, Andrews S R, Maier S A, Fernández-Domínguez A I, Martín-Moreno L and García-Vidal F J 2008 *Nat. Photon.* **2** 175
[35] Shen X P, Cui T J, Martin-Cano D and Garcia-Vidal F J 2013 *Proc. Natl. Acad. Sci. USA* **110** 40
[36] Yao H Z and Zhong S C 2014 *Opt. Express* **22** 25149
[37] Kim S H, Kim T T, Oh S S, Kim J E, Park H Y and Kee C S 2011 *Phys. Rev. B* **83** 165109
[38] Maier S A, Andrews S R, Martín-Moreno L and García-Vidal F J 2006 *Phys. Rev. Lett.* **97** 176805
[39] Maradudin A A, Simonsen I, Polanco J and Fitzgerald R M 2016 *J. Opt.* **18** 024004